Magneto-optical trap as an optical lattice

H. Schadwinkel, U. Reiter, V. Gomer, and D. Meschede

Institut für Angewandte Physik, Universität Bonn, Wegelerstrasse 8, D-53115 Bonn, Germany

We study the magneto-optical trap (MOT) as an optical lattice with a setup providing full phase control for all light fields. Although completely different light fields are possible for various phases, we have found experimental evidence that stored atoms are generally localized in micropotentials of the six-beam lattice. The influence of the phase variation is surprisingly small, suggesting that the robust behavior of the MOT is a consequence of this fact. We find furthermore good agreement of our experimental data with a simple theoretical model which reduces the complicated MOT to a description of steady-state atoms localized at points of the deepest adiabatic light-shift potential.

PACS number(s): 32.80.Pj, 42.50.Vk

Since its invention [1], the magneto-optical trap (MOT) has become the most important primary device for the preparation of a sample of cold atoms. It is now widely appreciated that even for moderate experimental conditions regarding laser intensities, beam quality or mechanical stability trapping and cooling of atoms is readily achieved. In a simple concept, the properties of the MOT are described by averaged radiation pressure forces which are spatially modified by a magnetic quadrupole field which also defines the center of the trapping volume [2]. While this ''restoring force and damping constant model'' description is acceptable at a more global scale, refined temperature measurements [3] and the observation of very narrow nonlinear resonances on the transmission of a weak probe beam [4,5] were connected to polarization gradient cooling mechanisms in periodic light-induced potentials [6,7]. The light interference pattern, however, strongly depends on the phase relations between the six trapping laser beams which are not controlled in the usual MOT experiments. This uncertainty was one of the reasons that after the first reported observation of narrow Raman resonances in MOTs [4,5], researchers switched to simpler one-dimensional (1D) light-field configurations with a clearly defined polarization state [8].

Spectroscopy of such specially constructed ''optical lattices'' (later also in two and three dimensions) exhibits narrow nonlinear resonances providing information about the localization and dynamics of atoms in optical micropotentials [8–10]. These techniques were also applied to the two-dimensional limit of a MOT operated with phase stable light fields by Hemmerich *et al.* [11]. The 2D limit shows a strong sensitivity of spatial confinement on the relative phases. Theoretical calculations also expect in general strong changes of the atomic dynamics as a function of the relative phases [12–14].

Drawing on both the experimental as well as the conceptual expertise developed with simple optical lattices [15,16], we are now in a position to show that atoms in a MOT are generally localized in light-shift potentials and that in contrast to expectations this fact is only weakly dependent on the relative phases of the three interfering standing waves. We compare these observations to a so-called ''good'' optical lattice, where the atoms are localized at points of circular

polarization. All experimental results are shown to agree well with calculations based on a no-free-parameter semiclassical model for the atom-light interaction.

Our experimental setup is identical with a standard six-beam magneto-optical trap, with the only exception being that the two relative time phases of the three contributing standing waves are intrinsically stable. The concept uses a single standing wave which is multiply folded and brought into triple intersection with itself. The relative phases of the three contributing standing waves can be adjusted by means of Faraday rotators. Details of this approach have been published elsewhere [17].

To be specific, we now define the laser beams through their wave vectors $\mathbf{k}_n$, polarizations ϵ_n, and phases ϕ_n so that the electric field takes the form $\mathbf{E}_L(\mathbf{r},t) = \mathcal{E}_0 \sum_n \epsilon_n e^{+i(\mathbf{k}_n \mathbf{r} + \phi_n)} e^{-i\omega_L t} + \text{c.c.}$ The six wave vectors correspond to the Cartesian directions $\mathbf{k}_{\pm \mathbf{x}} = \pm \mathbf{e_x} \cdots$ and the relative time phases are defined with respect to the z axis as $\Phi_x = \phi_x = \phi_{-x}$, $\Phi_y = \phi_y = \phi_{-y}$, and $\Phi_z \equiv 0 \equiv \phi_z \equiv \phi_{-z}$. The resulting light field depends on the phases Φ_x, Φ_y and polarizations ϵ_n. The circular polarizations of our MOT laser beams are generated by activating electro-optic switches to change the incoming polarizations from linear to circular $\epsilon_{\pm x}^{\text{MOT}} = (0, 1, \mp i), \epsilon_{\pm y}^{\text{MOT}} = (\mp i, 0, 1), \epsilon_{\pm z}^{\text{MOT}} = (1, \pm i, 0)$. A special case occurs for the $\text{MOT}_{\Phi_x = 0, \Phi_y = 0}$: The polarization is linear at all points as in a one-dimensional $\sigma^+ \sigma^-$ standing wave, but the intensity pattern is fully modulated (with eight intensity zeros per λ^3 unit cell). In the deactivated state of the electro-optic switches, the light configuration $\epsilon_{\pm x}^{\text{lin}} = (0, \pm 1, 1), \epsilon_{\pm y}^{\text{lin}} = (1, 0, \pm 1), \epsilon_{\pm z}^{\text{lin}} = (\pm 1, 1, 0)$ gives us immediate access to a three-dimensional generalization of the lin⊥lin [7] standing wave (3D lin⊥lin): For time phases $\Phi_x = 0, \Phi_y = 0$, the resulting interference pattern does not show any intensity variation apart from the envelope of the interfering laser beams. Instead, the polarization grating lattice is fully modulated from circular to linear. In this case one expects atoms to be well localized at points of circular polarization [18].

The trapping laser light field was drawn from a Ti-sapphire laser with frequency jitter less than 300 kHz with respect to the center of the cesium $D2$ line $F = 4 \rightarrow F' = 5$ transition. Repumping (for the $F = 3 \rightarrow F' = 4$ transition) and
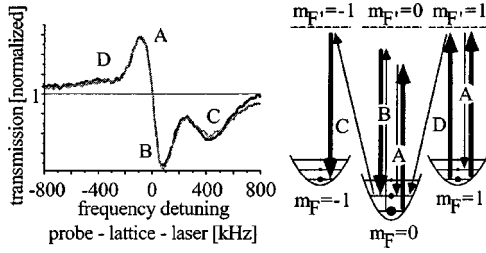
FIG. 1. Left: Transmission spectra for the $MOT_{0,0}$ light field for linear (gray) and circular probe polarization. For trapping laser parameters, $I=(3.8)I_S$ per beam, $\delta=(-5.3)\Gamma$, and the typical total absorption is 3–5 %. Right: Identification of the observed resonances (A)–(D). Thick arrows correspond to lattice photons and hence to π transitions due to our choice of quantization axis. Thin arrows correspond to π- as well as σ-polarized probe photons.

FIG. 2. Observed oscillator frequencies ν_{Osz} versus position of (C)-type transitions ν_C for $MOT_{0,0}$ and 3D lin$\perp$ lin$_{0,0}$ lattice (gray). Fitted lines correspond to square-root functions.

probe laser light was derived from diode lasers. The frequency of the probe laser was tuned to the vicinity of the trapping laser and controlled by a phase-locking technique [19] yielding sub kHz spectroscopic resolution in probe transmission measurements.

The experiment is computer controlled, allowing full variation of laser intensity, frequency offsets, and polarization state. The MOT is typically loaded with 10^7 atoms, at a red detuning δ of one natural linewidth Γ, an intensity of six times the saturation intensity $I_S=1.1$ mW/cm^2 in each beam, and at a magnetic-field gradient of 3 G/cm. The sample is then switched to the configuration under investigation and left to thermalize within 10 ms.

For transmission spectroscopy, a probe beam with weak intensity compared to the saturation intensity is focused through the trapped sample of atoms at a small ($\approx 10°$) angle to the z symmetry axis. Once the desired sample is prepared, a spectrum of the transmitted intensity is monitored within 100 ms, which is short compared to typical decay times of the trapped sample of order 1 s at a residual gas pressure of 5×10^{-10} mbar. Trapping laser intensity and detuning from the atomic resonance are varied between $I=(6-1.5)I_S$ and $\delta=(1-9)\Gamma$, respectively, implying a light-shift potential depth U_0 corresponding to 10^2-10^3 photon recoil energies E_R.

In Fig. 1 we show a characteristic spectrum in the immediate vicinity of the trapping laser frequency. Since in the $MOT_{0,0}$ the polarization is linear everywhere, its direction may be taken as the local quantization axis. The lowest optical potential then occurs for $m_F=0$, and Raman transitions between different vibrational levels are allowed as indicated by the letters (A)–(D). Since the local linear polarization can take on different orientations [20], both π and σ transitions are observed for both linear and circular probe polarization. The imbalance of transitions $\Delta m_F=-1$ (C) and $\Delta m_F=+1$ (D) is determined by the population difference of the sublevels, which is indicated by the sizes of the dots in Fig. 1.

In the case of the 3D lin$\perp$ lin light field, the general appearance of the spectrum (see Fig. 3) is similar to the $MOT_{0,0}$, in spite of the very different types of light fields. As the atoms are localized at points of pure circular polarization,
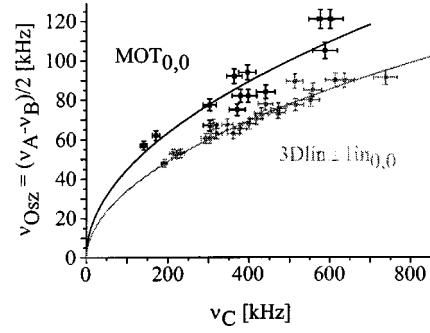
optical pumping populates only one sublevel which can be locally defined as $|m_F|=F=4$. This fact is responsible for the narrowing of spectral lines compared to the $MOT_{0,0}$ case, where various Raman transitions starting from different m_F sublevels contribute to the (A) and (B) resonances with slightly different resonance frequencies. In the 3D lin$\perp$ lin lattice, only the $|m_F|=4$ sublevel is populated and now even higher-order Raman transitions can be observed because the contributions starting from different vibrational levels have almost equal (besides the small potential anharmonicity) resonance frequencies.

Compared to the $MOT_{0,0}$ case, the (C)-type transition $|m_F|=4\rightarrow|m_F|=3$ now is more clearly separated from the $\Delta m_F=0$ transitions (A) and (B). This is due to the fact that the greater difference of Clebsch-Gordan coefficients induces a higher separation of sublevels $m_F=\pm4$ and $m_F=\pm3$ compared to $m_F=0$ and $m_F=\pm1$.

Our interpretation of the observed resonances is strongly supported by the dependence of the frequency difference of the gain (A) and the loss peak (B) on the position of the $|\Delta m_F|=1$ transition (C) as shown in Fig. 2. The observed square-root-type relation $\nu_{Osz}=\kappa\sqrt{\nu_C}$ suggests that for nearly harmonic optical potentials, the frequency difference $(\nu_A-\nu_B)/2$ is equal to ν_{Osz}, the frequency separation of the vibrational levels, while the position ν_C is a measure of the light-shift potential depth. The fitted values for κ allow quantitative comparison with our model (see below). The smaller jitter of experimental data for the 3D lin$\perp$ lin$_{0,0}$ spectra is due to its sharper morphology, which facilitates evaluation of the spectral line positions.

In order to model transmission spectra, we made the following simplifying assumptions: Trapped atoms are concentrated near locations of minimal potential energy induced by light shifts, and it is sufficient to study the atom light interaction at these points. In order to determine the location of lowest potential energy, we have computed the steady-state solution of the atomic ground-state density matrix, which is available in analytical form [21,22] for arbitrary angular momenta and light-field polarization. This gives us the populations of the various magnetic sublevels as well as their spatially varying light shifts. At the minima of the potentials their curvature yields the oscillation frequencies and hence the separation of the vibrational levels.
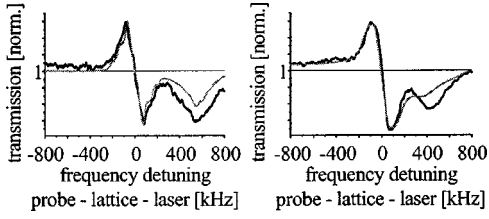
The transmission spectra depend furthermore on the

FIG. 3. Comparison of experimental and theoretical (gray) transmission spectra for two different light field configurations: 3D lin$\perp$lin$_{0,0}$ (left) and MOT$_{0,0}$ (right) at identical laser parameters as in Fig. 1.

FIG. 4. Left: Ellipticity of the local light field at the points of minimum potential energy as a function of time phases for MOT$_{\Phi_x,\Phi_y}$. The points (a)–(g) indicate the values of time phases where transmission spectra were recorded. Right: Experimental (gray) and theoretical oscillator frequencies ν_{Osz} for the time phase combinations (a)–(g).

population of oscillator levels Π_ν. Only 1D model calculations are available, but we have noticed that reported populations seem to depend little on angular momentum and show a remarkable insensitivity to the light shift for moderate intensities already (light shift $>50E_R$). We have therefore accepted the values $\Pi_0 \approx 0.35$, $\Pi_1 \approx 0.25$, $\Pi_2 \approx 0.15$, $\Pi_3 \approx 0.10, \ldots$ from Refs. [23–25] and inserted them into our calculation. Only for smaller light shifts does the assumption of constant populations seem not to be valid anymore, indicating that the number of bound vibrational levels is decreasing rapidly in that regime. This result can be connected to our observation that localization can hardly be observed for light shifts below $50E_R$, which is equivalent to $\Omega_{\text{Rabi}}^2/\delta\Gamma \lesssim 0.04$ and corresponds to $\nu_C \lesssim 200$ kHz in Fig. 2.

We do not explicitly take into account the polarization of the probe beam, since due to the high symmetry of the light fields there will always be σ as well as π transitions possible [20]. Each allowed transition is represented by a Lorentzian resonance curve weighted by the corresponding level populations with linewidths scaling as $\Gamma_{Osz} = \Gamma'(\nu + 1/2)\sqrt{E_R/U_0}$ [26], where Γ' is the optical pumping rate. Although this scaling law is usually applied to good optical lattices only, we would like to point out that equally narrow resonances can be observed in other light fields as well. This fact has been previously observed and explained for the case of π-polarized potential wells [27]. However, as there are always several transitions contributing to each of the resonances (A)–(D), the observed linewidth is determined by their frequency difference rather than by the width of the individual resonance curves.

An example of our calculation is shown in Fig. 3 for the MOT$_{0,0}$ and the 3D lin$\perp$lin$_{0,0}$ case. The better agreement of experimental and theoretical spectra in the latter case can be attributed to the much simpler lattice situation. But even for the MOT$_{0,0}$ light field, we can extract a theoretical coefficient κ relating oscillator frequencies and light shifts that deviates by only 14% from the experimental value. For the 3D lin$\perp$lin$_{0,0}$ lattice, the measured and calculated κ differ by 3% only.

In addition, very similar spectra were recorded for seven more different settings of the relative time phases of the MOT fields (see Fig. 4), indicating that in a regular magneto-optical trap full 3D localization of atoms occurs for all possible time phases. This observation differs substantially from Hemmerichs *et al.*'s [11] 2D experiment, in which only cer-
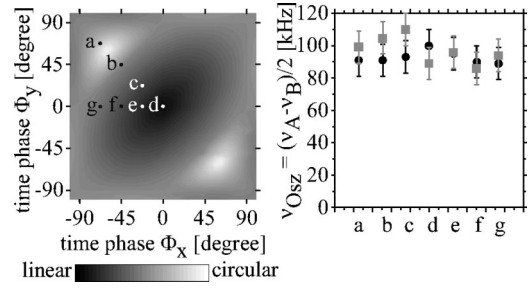
tain values of the relative time phases led to efficient localization. The difference with these experiments is further supported by the significantly smaller width obtained for the Raman resonances (100 kHz in our case versus 1 MHz), again indicating stronger confinement in all directions.

The reason for the weak dependence of the oscillation frequencies on the time phases is the interplay between polarization and intensity gradients of the 3D MOT light-field configuration. For example, in the case of $\Phi_{x,y} = \pm \pi/3$ [region near the point (a) in Fig. 4] the light field at the deepest potentials is circulary polarized, providing the maximum possible coupling of the local light field and the atoms optically pumped into the $|m_F| = F$ states. On the other hand, the strongest spatial intensity modulations take place for the MOT$_{0,0}$ case [point (d) in Fig. 4] with linear polarization everywhere. Hence the influence of the ellipticity on the light shift for various time phases is mostly compensated for by the intensity modulation of the corresponding light fields. As displayed in Fig. 4, the oscillation frequencies ν_{Osz} show only moderate variation of about 22% despite the obviously completely different light fields (a)–(g).

Our no-free-parameter model, which only employs laser intensity, detuning, and ellipticity of the local light field and assumes a model distribution of atoms among vibrational levels, reproduces experimental spectra with satisfactory accuracy regarding shape, position, and width of probe transmission resonances.

In conclusion, we propose to consider the low-temperature regime of the MOT as an optical lattice in the first place. A reconciliation with the spring constant model [2] may be obtained accounting for the different time scales used to derive information about the stored atoms. The transmission spectra reported here and in other works on optical lattices are typically governed by physical processes acting on the microsecond time scale. In contrast, the spring constant model which describes, for instance, position damping of an atom at length scales larger than the optical wavelength seems more appropriate on longer time scales of order milliseconds. This conclusion is in accord with our observation of different transport properties of a single atom in a MOT [28,29] by means of photon correlations, which also showed

a distinct behavior on the microsecond and millisecond scales.

[1] E.L. Raab *et al.*, Phys. Rev. Lett. **59**, 2631 (1987).

[2] C.G. Townsend *et al.*, Phys. Rev. A **52**, 1423 (1995).

[3] A.M. Steane and C.J. Foot, Europhys. Lett. **14**, 231 (1991).

[4] D. Grison *et al.*, Europhys. Lett. **15**, 149 (1991).

[5] J.W.R. Tabosa *et al.*, Phys. Rev. Lett. **66**, 3245 (1991).

[6] P.D. Lett *et al.*, Phys. Rev. Lett. **61**, 169 (1988).

[7] J. Dalibard and C. Cohen-Tannoudji, J. Opt. Soc. Am. B **6**, 2023 (1989).

[8] P. Verkerk *et al.*, Phys. Rev. Lett. **68**, 3861 (1992).

[9] A. Hemmerich, M. Weidemüller, and T. Hänsch, Laser Phys. **4**, 884 (1994).

[10] K.I. Petsas, A.B. Coates, and G. Grynberg, Phys. Rev. A **50**, 5173 (1994).

[11] A. Hemmerich *et al.*, Europhys. Lett. **21**, 445 (1993).

[12] K. Mølmer, Phys. Rev. A **44**, 5820 (1991).

[13] A.M. Steane, M. Chowdhury, and C.J. Foot, J. Opt. Soc. Am. B **9**, 2142 (1992).

[14] Y. Castin and K. Mølmer, Phys. Rev. Lett. **74**, 3772 (1995).

[15] G. Grynberg and C. Triché, in *Proceedings of the International School of Physics Enrico Fermi, Course CXXXI*, edited by A. Aspect, W. Barletta, and R. Bonifacio (IOS Press, Amsterdam, 1996), pp. 243–284.

[16] P. S. Jessen and I. Deutsch, in *Advances in Atomic, Molecular, and Optical Physics*, Vol. 37 of *Advances in Atomic, Molecular, and Optical Physics*, edited by B. Bederson and H. Walther (Academic Press, Cambridge, 1996), pp. 95–138.

[17] A. Rauschenbeutel *et al.*, Opt. Commun. **148**, 45 (1997).

[18] These circular polarizations do not occur at discrete points but on complicated interlaced lines.

[19] M. Prevedelli, T. Freegarde, and T.W. Hänsch, Appl. Phys. B: Lasers Opt. **60**, S241 (1995).

[20] In the $MOT_{0,0}$, for example, the atoms are localized at eight intensity antinodes in a unit cell. The directions of the local linear polarization at these points coincide with the diagonals $(\pm 1, \pm 1, \pm 1)$ of the coordinate system.

[21] A.V. Taǐchenachev, A.M. Tumaǐkin, and V.I. Yudin, Zh. Éksp. Teor. Fiz. **83** 1727 (1996) [JETP **83**, 949 (1996)].

[22] G. Nienhuis *et al.*, Europhys. Lett. **44**, 20 (1998).

[23] Y. Castin and J. Dalibard, Europhys. Lett. **14**, 761 (1991).

[24] Y. Castin, Ph.D. thesis, Université Paris VI, 1992.

[25] P. Marte *et al.*, Phys. Rev. Lett. **71**, 1335 (1993).

[26] J.-Y. Courtois and G. Grynberg, Phys. Rev. A **46**, 7060 (1992).

[27] C. Mennerat-Robillard *et al.*, Europhys. Lett. **38**, 429 (1997).

[28] V. Gomer *et al.*, Phys. Rev. A **58**, R1657 (1998).

[29] H. Schadwinkel *et al.* (unpublished).